Nucleation of Ga Droplets Self-Assembly on GaAs(111)A Substrates

Artur Tuktamyshev (a.tuktamyshev@campus.unimib.it)
University of Milano-Bicocca
Alexey Fedorov
Istituto di Fotonica e Nanotecnologie
Sergio Bietti
University of Milano-Bicocca
Stefano Vichi
University of Milano-Bicocca
Riccardo Tambone
University of Milano-Bicocca
Shiro Tsukamoto
University of Milano-Bicocca
Stefano Sanguinetti
University of Milano-Bicocca

Research Article

Keywords: self-assembled quantum dots (QDs), GaAs(111)A Substrates

Posted Date: February 3rd, 2021

DOI: https://doi.org/10.21203/rs.3.rs-199999/v1

Version of Record: A version of this preprint was published at Scientific Reports on March 25th, 2021. See the published version at https://doi.org/10.1038/s41598-021-86339-3.

Nucleation of Ga Droplets Self-Assembly on GaAs(111)A Substrates

Artur Tuktamyshev[1,*], Alexey Fedorov[2], Sergio Bietti[1], Stefano Vichi[1], Riccardo Tambone[1], Shiro Tsukamoto[1], and Stefano Sanguinetti[1]

[1]L-NESS and Department of Material Science, University of Milano-Bicocca, via R. Cozzi 55, 20125 Milano, Italy
[2]L-NESS and CNR–IFN, Polo di Como, via F. Anzani 42, 22100 Como, Italy
[*]a.tuktamyshev@campus.unimib.it

ABSTRACT

We investigated the nucleation of Ga droplets on singular GaAs(111)A substrates in the view of their use as the seeds for the self-assembled droplet epitaxial quantum dots. A small critical cluster size of 1–2 atoms characterizes the droplet nucleation. Low values of the Hopkins-Skellam index (as low as 0.35) demonstrate a high degree of a spatial order of the droplet ensemble. Around 350 °C the droplet size distribution becomes bimodal. We attribute this observation to the interplay between the local environment and the limitation to the adatom surface diffusion introduced by the Ehrlich-Schwöbel barrier at the terrace edges.

Introduction

The unique properties of the self-assembled quantum dots (QDs), such as the discrete energy levels and a precise control of additional features, like entangled photon emission, by the QD shape and size, have a great potential in the optoelectronic device fabrication for the future quantum network applications[1–4]. For this reason, one of the main challenges in the QD self-assembly is the reproducibility of QDs in terms of shape and size.

Droplet epitaxy (DE) is well-established for the formation of III-V compound semiconductor nanostructures and allows to control the QD density and size in a wide range[5,6]. The size distribution of the self-assembled DE QDs is strictly determined by the original size distribution of the droplets[7]. As the droplet size distribution can be easily controlled, using DE technique, it is then possible to obtain a narrow QD size distribution, resulting in a small ensemble photoluminescence linewidth[8].

The QD self-assembly on (111) surfaces is complex using the Stranski-Krastanov (SK) growth mode[9] (only recently the self-assembly of SK QDs on the (111)A surface was demonstrated[10,11] by taking profit of tensile strain). Nevertheless, DE allows to the density and the size control of the self-assembled QDs on (111) surfaces, thus exploiting the C_{3v} symmetry of the surface, to obtain highly symmetric QDs[12–14]. Recently, the studies of shape-controlled highly symmetric DE GaAs QDs grown on AlGaAs/GaAs(111)A[14] for entangled photon pair generation[13] have been published.

In this work, we investigated the Ga droplet self-assembly on singular GaAs(111)A substrates in order to gain fundamental understanding of the effects of the surface characteristics, in terms of a surface reconstruction and a morphology, on the island nucleation dynamics. The droplet density dependence on the temperature has been determined in the temperature range between 300 and 450 °C. This gave us access to the fundamental physical quantities which determine the droplet formation dynamics: 1) the critical nucleus size for the droplet formation[15,16]; 2) the adatom surface diffusivity and its dependence on the surface reconstruction. We have also investigated the effect of surface defects on the droplet size distribution in combination with the presence of the sizeable Ehrlich-Schwöbel barrier typical for the GaAs(111)A surface[17].

Methods

The samples were grown, using a molecular beam epitaxy (MBE) system, on an undoped singular GaAs(111)A substrates. The substrate temperature was measured by the thermocouple situated between the substrate heater and the sample, and by the infrared pyrometer.

After an oxide desorption at 590 °C, a 50 nm GaAs buffer layer was deposited at the temperature of 520 °C with a deposition rate of 0.07 ML/s (here and below 1 ML is defined as 6.26×10^{14} atoms/cm^2, which is the site-number density of the unreconstructed GaAs(001) surface), in order to obtain a smooth surface[17]. The substrate temperature was then decreased to the droplet deposition temperature varying from 300 to 450 °C. During the droplet deposition the As cell valve was closed in order to deplete the growth chamber from the arsenic molecules. 2 ML of gallium were deposited at a rate of 0.01 ML/s. During the Ga deposition, the background pressure was below 3×10^{-9} torr. The supply of Ga without As_4 enabled the appearance of the

Ga liquid droplets on the buffer layer surface. Next, an As_4 flux with a beam equivalent pressure (BEP) of 6.2×10^{-5} torr was supplied at the same temperature for 3 minutes, in order to crystallize Ga droplets into GaAs islands. The sample T2b was arsenized after 30 minutes of annealing of Ga droplets at 350 °C, in order to study the influence of the ripening processes on the island density and size.

As shown in Refs.[18–20], the density of DE QDs, when crystallized at the same temperature used for the deposition of the metal droplets, mirrors that of droplets, thus making possible to access the density dependence of Ga droplets on the deposition parameters through the measurement of the island density. The crystallized surface morphology is more stable on time and avoids the strong oxidation effects which would hinder the reproducibility of the atomic force microscope (AFM) measurements.

The *ex-situ* morphological characterization of the samples was performed by AFM in a tapping mode, using tips capable of a lateral resolution of about 2 nm.

The growth description of the samples is summarized in Table 1.

Sample	***T*, °C**	***N*, cm^{-2}**	**Comments**
T1	300	$(7.67\pm1.15)\times10^{10}$	
T2	350	$(1.83\pm0.06)\times10^{10}$	
T2b	350	$(1.85\pm0.09)\times10^{10}$	Arsenization after 30 minutes annealing
T3	400	$(2.27\pm0.05)\times10^{9}$	
T4	450	$(7.17\pm1.08)\times10^{8}$	

Table 1. The substrate temperature during the Ga droplet nucleation and the subsequent arsenization of the samples, presented in this work as well as the GaAs island density of the samples.

Results and Discussion

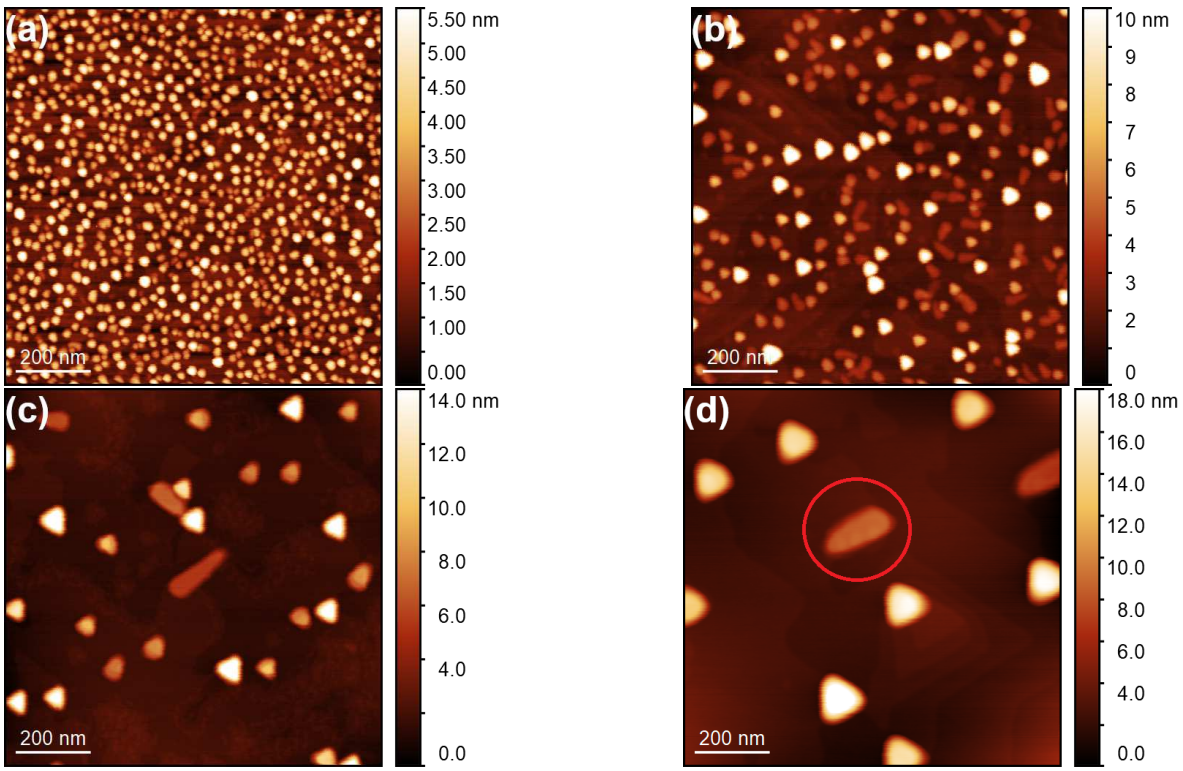

Figure 1. AFM topography images of GaAs islands grown on the GaAs(111)A substrate at (a) 300 °C (1×1 μm^2, sample T1); (b) 350 °C (1×1 μm^2, sample T2); (c) 400 °C (1×1 μm^2, sample T3); (d) 450 °C (1×1 μm^2, sample T4). The red circle highlights a kinked island.

Figure 1 shows AFM images of the samples T1, T2, T3, and T4 with GaAs islands, grown at 300, 350, 400, and 450 °C, respectively. As expected, with increasing the deposition temperature the island density decreases[18–21]. This tendency satisfies the classical nucleation theory of J. A. Venables[15,16], which describes a nucleation of Ga droplets as a thermally activated process. As a result, the density of droplets N is reproduced by the Arrhenius law:

$$N \propto exp(E_a/k_BT), \tag{1}$$

where E_a is the nucleation activation energy, k_B – the Boltzmann's constant, and T is the Ga droplet deposition temperature.

It is worth to mention that some of DE GaAs islands, grown on a singular GaAs(111)A surface, are "kinked" (Ga droplets are spontaneously crystallized in a horizontal direction). One kinked dot is highlighted on Figure 1d. The analogues of such islands are kinked nanowires (NWs) performed by the vapor-liquid-solid (VLS) growth on (111) surfaces[22–24]. The growth in a horizontal direction and a subsequent formation of kinked NWs is induced by a twin-mediated mechanism, which can be suppressed/maintained by controlling the growth conditions[23,24]. This behavior of a spontaneous nucleation of kinked GaAs islands on singular GaAs(111)A surface is in agreement with the expected island formation during the crystallization (arsenization) process of Ga droplets under the VLS mechanism.

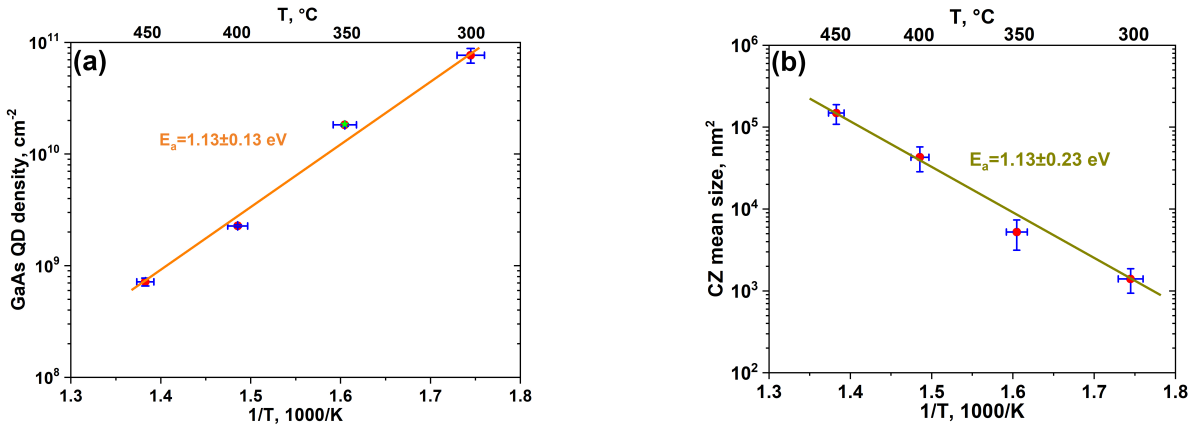

Figure 2. (a) The temperature density dependence of DE GaAs islands grown on GaAs(111)A substrate. The green star indicates the island density of the sample T2b. The nucleation activation energy, E_a = 1.13±0.13 eV. (b) The temperature dependence of a mean size of Voronoi cells. The activation energy E_a, calculated from this method, equals 1.13±0.23 eV. The temperature error bar for both graphs is ±5 °C.

Using the Arrhenius plot of the density dependence on the deposition temperature, it is possible to calculate the activation energy E_a. Figure 2a shows the temperature density dependence of GaAs islands in the range of 300 – 450 °C. The temperature error bar in our measurements is associated with the accuracy of the substrate temperature determination by the thermocouple and equals roughly ±5 °C. The density calculation was carried out using the data of several AFM scans from different areas of the samples. The density ranges from 7×10^8 cm^{-2} to 8×10^{10} cm^{-2}. The activation energy, calculated from the temperature dependence of the island density, is 1.13±0.13 eV. This value is in between the ones, which we calculated for the Ga droplet nucleation on vicinal GaAs(111)A[20]. It is assumed that the the Ga droplet nucleation on singular GaAs(111)A is characterized by both types of diffusion (one- and two-dimensional).

A drastic change in the slope of the Arrhenius plot at T > 200 °C was observed previously for the temperature density dependence of DE GaAs islands grown on GaAs(001)[18] and Ga droplets on singular GaAs(111)A[21]. Such a phenomenon was attributed to the onset of the Ostwald ripening process (the growth of large clusters on the cost of smaller ones and hence a decrease of the total cluster density in a closed thermodynamic system[25]) with increasing the deposition temperature. Such a change of the Arrhenius slope was not observed in the present work. In order to check the presence of the Ostwald ripening, we prepared the sample T2b, for which the arsenization process was carried out after 30 minutes of an annealing process at the same temperature. The island density of the sample equals $(1.85\pm0.09)\times10^{10}$ cm^{-2} (the green star on Figure 2a). The value is only slightly higher than that observed in the sample T2 – $(1.83\pm0.06)\times10^{10}$ cm^{-2}, for which the annealing was not performed. This suggests that no Ostwald ripening occurs after the deposition of Ga droplets in our experiments.

Additionally, the characteristic parameters of the nucleation process such as the activation energy E_a and the size of stable cluster i (the number of atoms that are the part of the largest unstable cluster[15,16]) can be obtained from the capture zone distribution (CZD) approach[20,26,27].

Figure 2b shows the temperature dependence of a mean size of Voronoi cells for the samples T1, T2, T3, and T4. Naturally, the total number of Voronoi cells are related to the island density, so using this dependence, it is also possible to determine E_a. From the CZD approach E_a = 1.13±0.23 eV, which is in agreement with the value determined from the island density dependence.

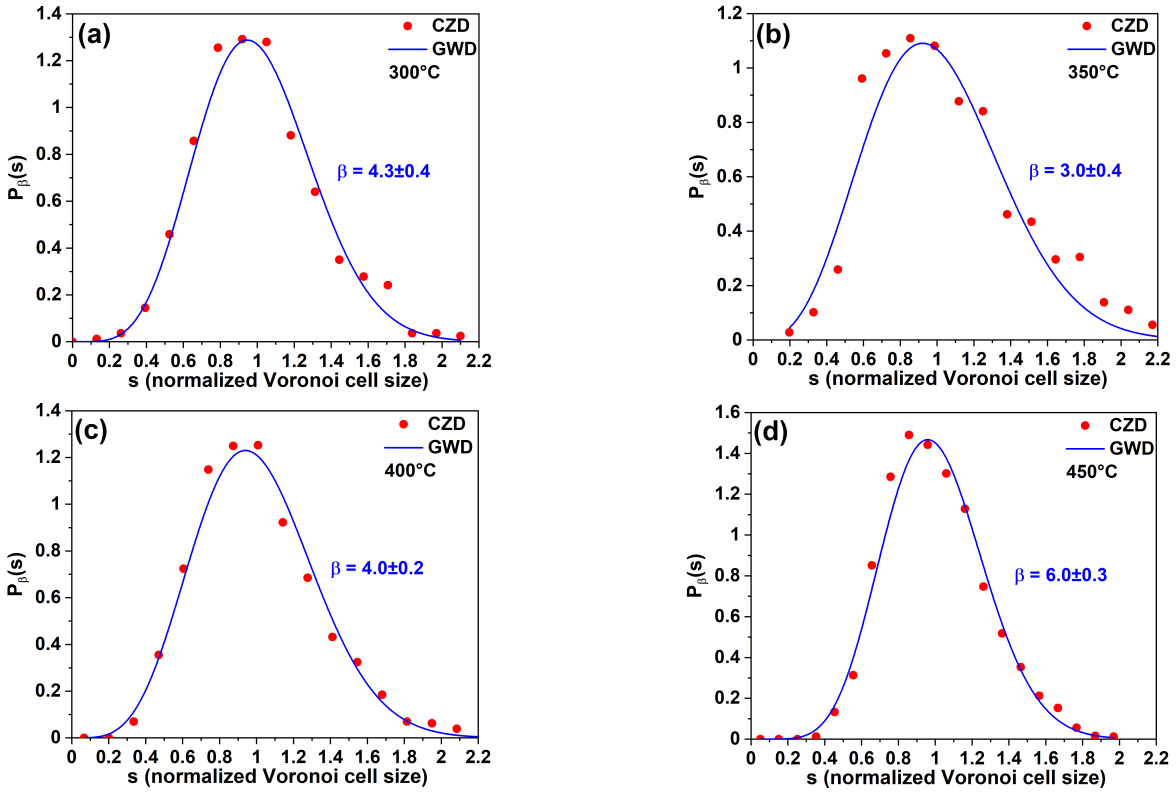

Figure 3. CZDs of the samples (a) T1, (b) T2, (c) T3, and (d) T4, fitted by the GWD.

In order to determine the critical cluster size i, we analyzed normalized (to the mean size of Voronoi cells) CZD from the Voronoi tessellation and fitted the CZD by the generalized Wigner distribution (GWD)[20,26,27] (see Figure 3):

$$P_\beta(s) = a_\beta s^\beta exp(-b_\beta s^2), \tag{2}$$

where s is the capture zone (CZ) area divided by its average value, a_β and b_β are the constants that assure the normalization and the unit mean conditions, respectively.

The fitting parameter β depends on i and the dimensionality of the diffusion γ as[20,27]

$$\beta = \gamma i + \gamma + i. \tag{3}$$

Sample	β	$i = \beta$ - 2
T1 (300 °C)	4.3±0.4	2.3±0.4
T2 (350 °C)	3.0±0.4	1.0±0.4
T3 (400 °C)	4.0±0.2	2.0±0.2
T4 (450 °C)	6.0±0.3	4.0±0.3

Table 2. The fitting parameter β and the critical cluster size i of the samples T1, T2, T3, and T4.

The parameter β and the critical cluster size i obtained with γ = 1 (taking into account a two-dimensional adatom diffusion[20,27]) are presented in Table 2. For T $\leq$ 400 °C the critical cluster size for the Ga droplet nucleation on singular

GaAs(111)A i = 1–2 atoms, which is in good agreement with the previous studies[20,21]. We observed an increase of the critical cluster size at 450 °C, which is compatible with the expected stable cluster decomposition due to the thermally activated atom detachment processes[15,16].

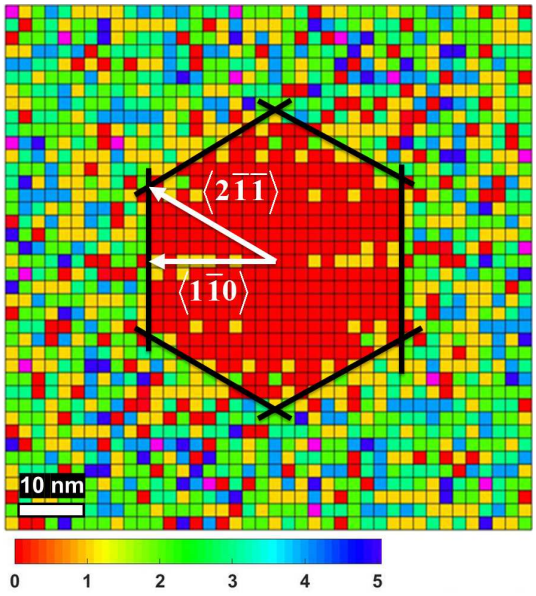

Figure 4. The spatial neighbor distribution of GaAs islands for the sample T1 (80×80 nm^2).

The diffusivity behavior of Ga adatoms can be monitored through the spatial neighbor distribution of islands[20]. The spatial dispersion of the neighboring GaAs islands for the sample T1 is presented in Figure 4. The distribution represents the position of the neighboring dots around the selected one in a small area (80×80 nm^2 in that case) taking into account all dots in the 1×1 μm^2 AFM scan. Therefore, such a distribution is a two-dimensional histogram of the neighboring dots and the small colored squares represent bins of the histogram. The other samples show similar distribution, but with less statistics, since the island density is higher at lower deposition temperature. The average excluded area (the area without the neighboring islands) has an almost symmetrical, nearly hexagonal, shape with the vertices in the $< 2\bar{1}\bar{1} >$ directions. The shape of the excluded zone suggests that $< 2\bar{1}\bar{1} >$ directions are preferable for the Ga adatom diffusion on GaAs(111)A. This observation is in agreement with the Ga-vacancy (2×2) surface reconstruction of GaAs(111)A[28,29]. According to Ref.[29], the diffusion activation energies E_d equal 1.06 and 1.14 eV for Ga adatom diffusion in the $< 2\bar{1}\bar{1} >$ and $< 1\bar{1}0 >$ directions, respectively, on the GaAs(111)A-(2×2) surface reconstruction. Thus, the diffusion length in the $< 2\bar{1}\bar{1} >$ directions should be longer, which we observed from the excluded zone area.

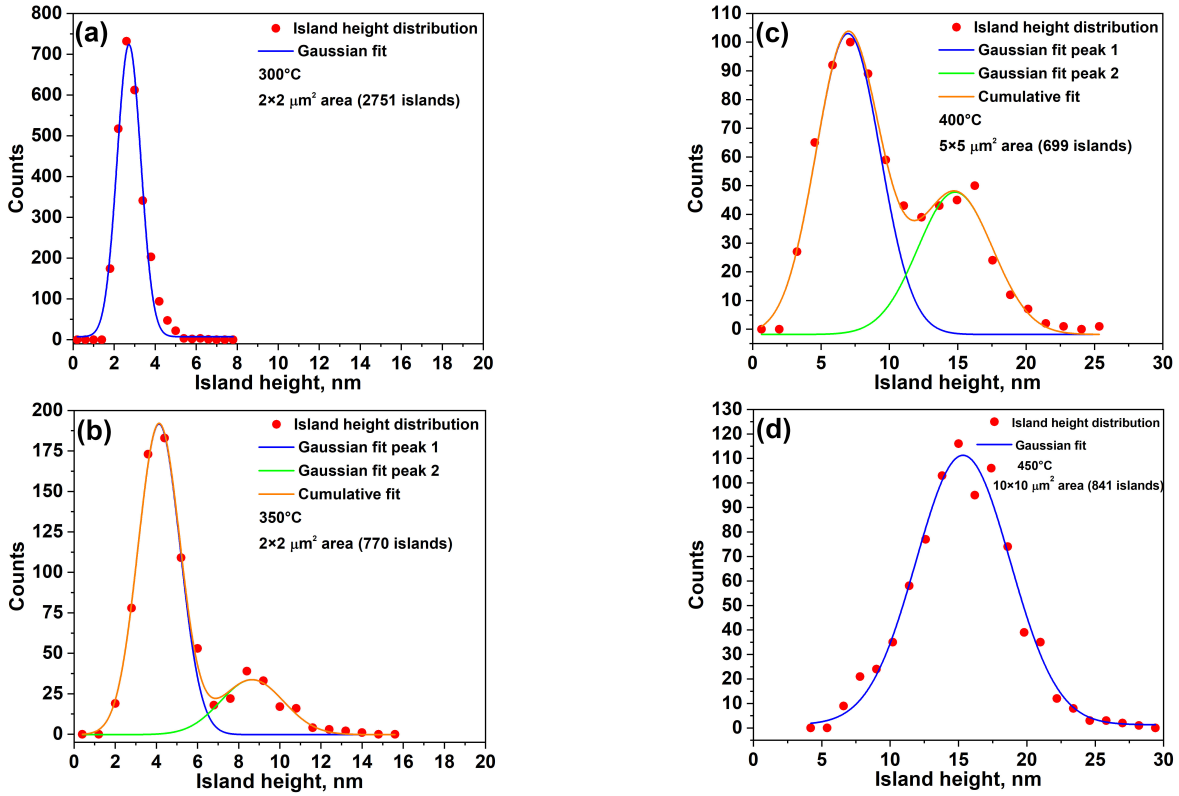

Figure 5. The GaAs island height distribution of samples (a) T1, (b) T2, (c) T3, and (d) T4. For the samples T1 and T4 an unimodal distribution is observed with a standard deviation of about 44%. The samples T2 and T3 have a bimodal distribution.

The last goal of this work is to study a size distribution of the grown islands. Figure 5 shows the GaAs island height distribution of the samples T1, T2, T3, and T4 fitted by the Gaussian line shapes. At the low deposition temperature of 300 °C the size distribution has a mean island height of about 2.7 nm with a standard deviation of 43% (Figure 5a). Similar situation at the high temperature of 450 °C (Figure 5d). The mean height for the sample T4 is about 15.3 nm with the standard deviation of 45%. And the most intriguing observation is the presence of a bimodal island size distribution at the intermediate temperatures (350 – 400 °C). The sample T2 (Figure 5b) has two groups of islands with the mean heights of 4.1 and 8.7 nm. And the mean island heights for sample T3 (Figure 5c) are 7.0 and 14.8 nm. For both cases the aspect ratio R (the height over the base) of bigger islands is approximately two times larger than the one of smaller islands.

The most known systems, where the bimodal QD size distribution was observed, are SK InAs/GaAs(001) QDs[30–33], where the bimodal behavior was described in terms of InAs coverage[31,32], which is the distinct threshold for the SK dot formation, and SK Ge/Si(001) islands[34,35], for whom the morphological shape transition of Ge islands is responsible for the bimodal distribution.

In order to study the origin of the bimodal size distribution in our samples, we investigated the degree of order of the droplet spatial arrangement which can be determined via the Hopkins-Skellam index (I_{HS}) of the droplet ensemble[36,37]. I_{HS} permits a precise measurement of a spatial regularity of the droplet distribution through the comparison with a purely random spatial distribution of the ensemble elements. I_{HS} is defined as

$$I_{HS} = \frac{\sum_{i=1}^{N} r_{1i}^2}{\sum_{i=1}^{N} r_{2i}^2}, \tag{4}$$

where N is the total number of droplets. The term r_{1i}^2 represents the distance to the nearest droplet from a random location in the studied area. Similarly, r_{2i}^2 denotes the distance to the nearest droplet from the *i-th* droplet. Therefore, for a completely random distribution (Poisson) of droplets, $I_{HS} = 1$. A droplet pattern which shows a clusterization returns a value $I_{HS} > 1$. The minimum value of I_{HS} is obtained for a perfectly ordered pattern of droplets, such as the hexagonal lattice, which gives $I_{HS} = 0.14$. Therefore, for the patterns with an intermediate regularity, the value of I_{HS} is expected to be framed between 0.14 to 1, with the I_{HS} value increasing with the disorder.

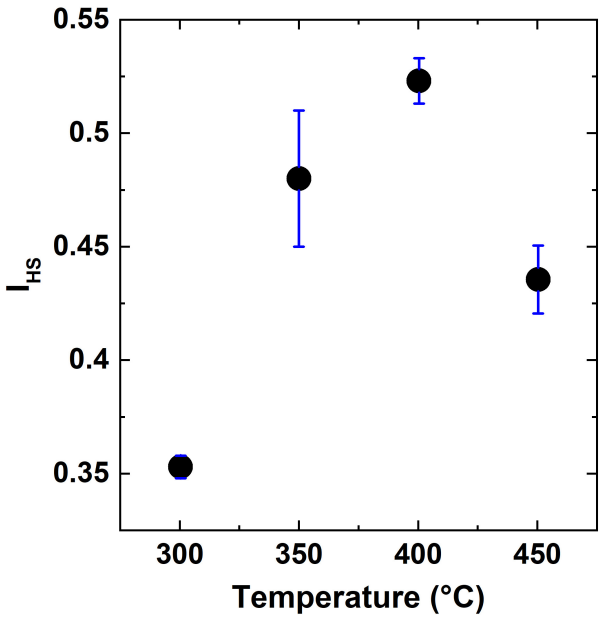

Figure 6. The dependence of the Hopkins-Skellam index (I_{HS}) on the deposition temperature.

The dependence of I_{HS} on the deposition temperature is reported in Figure 6. At low temperatures, the droplets, although randomly located, show a high degree of order, with $I_{HS} = 0.35$, thus closer to a regular lattice than to a random ensemble. As the temperature reaches the onset of the bimodal distribution (T = 350°C), the Hopkins-Skellam index steeply increases to $I_{HS} \approx 0.5$. A marked dependence on the position on the sample is also observed. The droplet distribution regains a partial order only at T = 450 °C, where $I_{HS} = 0.43 \pm 0.01$. Thus, the presence of the bimodal distribution of size walks together with a sizeable decrease of a droplet spatial order, which depends on the location on the sample surface.

As already mentioned, we do not observe ripening processes of Ga droplets. Therefore, the bimodal behavior at the intermediate temperature should stems from a different process able to produce multimodal and broad island size distribution. Together with the Hopkins-Skellam analysis of the spatial arrangement of the droplets, this calls for the presence of a temperature activated extrinsic nucleation process, sensible to the local environment, and affecting the growth kinetics of the droplets in the 350 –– 400 °C temperature range only.

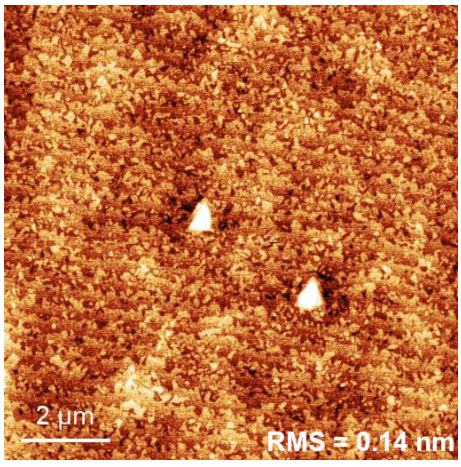

Figure 7. $10 \times 10\ \mu m^2$ AFM amplitude image of GaAs buffer layer morphology, grown according to Ref.[17] and used in this work.

A highly flat and smooth surface was obtained using rather low growth rate and high V/III ratio following the prescription of Ref.[17]. This prevents the formation of large (with μm lateral dimensions) triangular pyramidal hillocks consisting of up to several tens of steps, nucleated by the staking faults[38]. The surface morphology of our samples before the droplet deposition is

presented on Figure 7. The surface is very smooth with a root-mean-square (RMS) roughness of only 0.14 nm. Nevertheless, small hillocks consisting of several steps are still present (see e.g. Figure 8a, where the stepped triangular pyramid with 4 — 5 steps is observable inside the area highlighted with the blue lines). The hillocks, thus, introduce a sizeable density of steps on an otherwise nearly free singular GaAs(111)A surface.

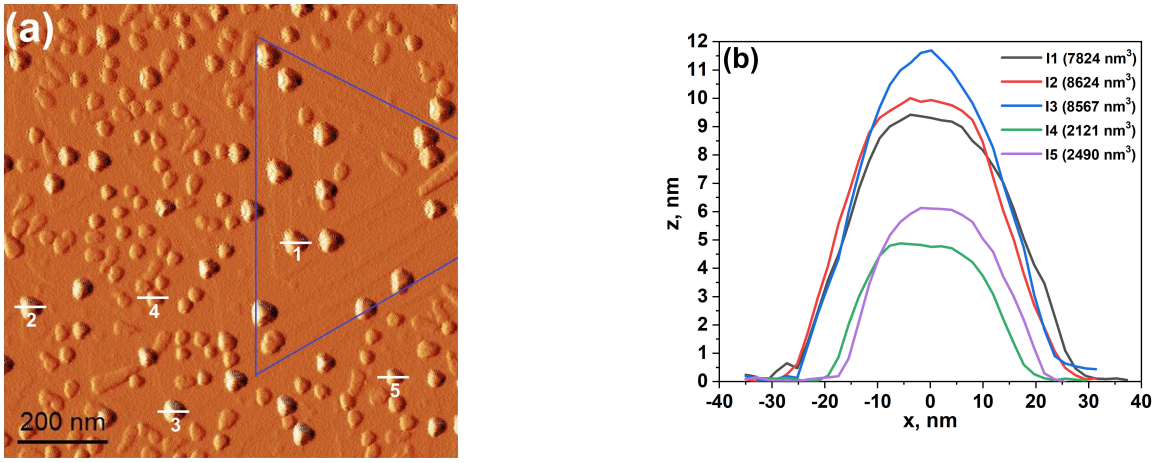

Figure 8. (a) 1×1 μm^2 AFM amplitude image of the sample T2. The white lines indicate where the height profiles of islands were measured. The blue lines indicate the area of the stepped hillock. (b) The height profiles of 5 islands of the sample taken from (a).

We then analyzed the local surface morphology for different island size in the sample T2 (see Figure 8a). The height profiles of five randomly chosen islands are presented in Figure 8b. The maximum height of islands I1-I3 (which belong to the large droplet mode) is about 9 — 12 nm. On the contrary the maximum height of the small islands I4-I5 is only 5 -– 6 nm. Taking also into account the slight change in island radius, the big islands show a volume which is roughly four times larger than the one of the small islands. By analyzing the local environment of the islands, we found that the islands originated from the small droplets which are nucleated within flat terrace areas. On the contrary, the large islands from the large droplets are always nucleated at the step edges joining two terraces.

The original surface morphology affects on the droplet size distribution and thus, in turn the island size. Combining this observation with the finite temperature range where the bimodal distribution is observed, we can interpret the relationship between the local environment and the droplet size as stemming from the combined effect of the initial droplet nucleation site and the influence of the presence of ES barrier at the step edges on the adatom diffusion length[17,20,39].

As a matter of fact, the droplets grow by capturing adatoms roughly within a diffusion length distance from the droplet itself. At low temperature the adatom diffusion length ℓ_D is small, compared to the average terrace width W_T. So, the presence of the ES barrier, which limits the adatom diffusion perpendicularly to the steps, is not affecting the adatom capture kinetics. The actual environment of the nucleation site is not playing a fundamental role at low T, and a unimodal behavior is predicted. As the temperature increases, the diffusion length increases until $\ell_D > W_T$. However, the presence of a sizable ES barrier limits the adatom CZ of each droplet within the terrace where the droplet is located. This introduces a broadening effect in the island size which has a marked local dependence, as it depends on the actual terrace width on which the droplet nucleated. In particular, the origin of the bimodal distribution of height is related to the observation that the droplets, nucleated at terrace edges, can collect adatoms from the two contiguous terraces. As the temperature further increases, the droplet CZ size is no more affected by the presence of finite width terraces, as the ES barrier at the step edges can be overcome by adatoms. This makes the CZ size independent from the local environment, thus restoring the unimodal size distribution of the island size.

Conclusions

Ga droplet nucleation dynamics on singular GaAs(111)A substrates, that we analyzed through the CZD approach[26,27], is characterized by a small critical nucleus size i = 1–2 atoms. This finding supports the recent critical cluster determination by Ohtake et al.[21] based on the droplet density dependence on metal flux. It shows that lower reactivity of GaAs(111)A, respect to GaAs(001), permits the stabilization of smaller predicted magic Ga cluster, constituted by just three atoms[40]. On the contrary, larger i is observed on GaAs(001) substrates[40,41]. The single activation energy for the droplet density dependence on the temperature (E_a = 1.13±0.23 eV) is observed in the whole measured range. At low and high temperature the spatial distribution

of the droplets on the surface is remarkably regular, with a HS index $I_{HS} = 0.35$, thus approaching that of the hexagonal lattice ($I_{HS} = 0.14$). The average excluded area around each island is highly symmetrical, with a nearly hexagonal shape with the vertices in $< 2\bar{1}\bar{1} >$ directions. The shape of the excluded zone suggests that $< 2\bar{1}\bar{1} >$ directions are preferable for Ga adatom diffusion on GaAs(111)A. This observation is in agreement with Ga-vacancy (2×2) surface reconstruction of GaAs(111)A[28,29].

At intermediate temperatures (350 – 400 °C) we observe the bimodal size distribution of GaAs islands, connected with a sharp increase of the disorder of the island sites, as measured by the HS index. At $T = 400$ °C, $0.45 < I_{HS} < 0.55$, with a marked dependence on the sample site. We attributed such behavior to the influence of local surface morphology which is sampled by the island CZ during its growth. Wide terraces (tens of nm wide) are observed on the singular GaAs(111)A surface and related to the presence of large and flat hillocks generated by the stacking faults[17,38,39]. The bimodal size distribution is attributed to the presence of the strong ES barrier at the terrace step edges[17], which limits Ga adatom diffusion on the terraces, thus inducing strong differences in the CZ size for droplets are nucleated on the terraces or at the terrace step edges. The same effect is responsible of the increase of I_{HS} index and the local variation.

References

1. Liu, A. Y. *et al.* High performance continuous wave 1.3 μm quantum dot lasers on silicon. *Appl. Phys. Lett.* **104**, 041104, DOI: https://doi.org/10.1063/1.4863223 (2014).
2. Stiff-Roberts, A. D. Quantum-dot infrared photodetectors: a review. *J. Nanophotonics* **3**, 031607, DOI: https://doi.org/10.1117/1.3125802 (2009).
3. Beattie, N. S. *et al.* Quantum engineering of InAs/GaAs quantum dot based intermediate band solar cells. *ACS Photonics* **4**, 2745–2750, DOI: https://doi.org/10.1021/acsphotonics.7b00673 (2017).
4. Huber, D., Reindl, M., Aberl, J., Rastelli, A. & Trotta, R. Semiconductor quantum dots as an ideal source of polarization-entangled photon pairs on-demand: a review. *J. Opt.* **20**, 073002, DOI: https://doi.org/10.1088/2040-8986/aac4c4 (2018).
5. Koguchi, N., Ishige, K. & Takahashi, S. New selective molecular beam epitaxial growth method for direct formation of GaAs quantum dots. *J. Vac. Sci. Technol. B* **11**, 787–790, DOI: https://doi.org/10.1116/1.586789 (1993).
6. Gurioli, M., Wang, Z., Rastelli, A., Kuroda, T. & Sanguinetti, S. Droplet epitaxy of semiconductor nanostructures for quantum photonic devices. *Nat. Mater.* **18**, 799–810, DOI: https://doi.org/10.1038/s41563-019-0355-y (2019).
7. Watanabe, K., Tsukamoto, S., Gotoh, Y. & Koguchi, N. Photoluminescence studies of GaAs quantum dots grown by droplet epitaxy. *J. Cryst. Growth* **227-228**, 1073–1077, DOI: https://doi.org/10.1016/S0022-0248(01)00991-5 (2001).
8. Basso Basset, F. *et al.* Spectral broadening in self-assembled GaAs quantum dots with narrow size distribution. *J. Appl. Phys.* **126**, 024301, DOI: https://doi.org/10.1063/1.5097277 (2019).
9. Chen, J. X. *et al.* Tuning InAs/GaAs quantum dot properties under Stranski-Krastanov growth mode for 1.3 μm applications. *J. Appl. Phys.* **91**, 6710–6716, DOI: https://doi.org/10.1063/1.1476069 (2002).
10. Schuck, C. F. *et al.* Self-assembly of (111)-oriented tensile-strained quantum dots by molecular beam epitaxy. *J. Vac. Sci. Technol. B* **36**, 031803, DOI: https://doi.org/10.1116/1.5018002 (2018).
11. Schuck, C. F. *et al.* Anomalous Stranski-Krastanov growth of (111)-oriented quantum dots with tunable wetting layer thickness. *Sci. Reports* **9**, 18179, DOI: https://doi.org/10.1038/s41598-019-54668-z (2019).
12. Jo, M. *et al.* Self-limiting growth of hexagonal and triangular quantum dots on (111)A. *Cryst. Growth Des.* **12**, 1411–1415, DOI: https://doi.org/10.1021/cg201513m (2012).
13. Basso Basset, F. *et al.* High-yield fabrication of entangled photon emitters for hybrid quantum networking using high-temperature droplet epitaxy. *Nano Lett.* **18**, 505–512, DOI: https://doi.org/10.1021/acs.nanolett.7b04472 (2018).
14. Bietti, S. *et al.* High–temperature droplet epitaxy of symmetric GaAs/AlGaAs quantum dots. *Sci. Reports* **10**, 6532, DOI: https://doi.org/10.1038/s41598-020-62248-9 (2020).
15. Venables, J. A., Spiller, G. D. T. & Hanbucken, M. Nucleation and growth of thin films. *Reports on Prog. Phys.* **47**, 399–459, DOI: https://doi.org/10.1088/0034-4885/47/4/002 (1984).
16. Venables, J. A. Atomic processes in crystal growth. *Surf. Sci.* **299/300**, 798–817, DOI: https://doi.org/10.1016/0039-6028(94)90698-X (1994).
17. Esposito, L., Bietti, S., Fedorov, A., Nötzel, R. & Sanguinetti, S. Ehrlich-Schwöbel effect on the growth dynamics of GaAs(111)A surfaces. *Phys. Rev. Mater.* **1**, 024602, DOI: https://doi.org/10.1103/PhysRevMaterials.1.024602 (2017).
18. Heyn, C. *et al.* Regimes of GaAs quantum dot self-assembly by droplet epitaxy. *Phys. Rev. B* **76**, 075317, DOI: https://doi.org/10.1103/PhysRevB.76.075317 (2007).

19. Fuster, D. *et al.* InAs nanostructures grown by droplet epitaxy directly on InP(001) substrates. *J. Cryst. Growth* **434**, 81–87, DOI: https://doi.org/10.1016/j.jcrysgro.2015.11.003 (2016).

20. Tuktamyshev, A., Fedorov, A., Bietti, S., Tsukamoto, S. & Sanguinetti, S. Temperature activated dimensionality crossover in the nucleation of quantum dots by droplet epitaxy on GaAs(111)A vicinal substrates. *Sci. Reports* **9**, 14520, DOI: https://doi.org/10.1038/s41598-019-51161-5 (2019).

21. Ohtake, A., Ha, N. & Mano, T. Extremely high- and low-density of Ga droplets on GaAs{111}A,B: surface-polarity dependence. *Cryst. Growth Des.* **15**, 485–488, DOI: https://doi.org/10.1021/cg501545n (2015).

22. Tian, B., Xie, P., Kempa, T. J., Bell, D. C. & Lieber, C. M. Single-crystalline kinked semiconductor nanowire superstructures. *Nat. Nanotechnol.* **4**, 824–829, DOI: https://doi.org/10.1038/nnano.2009.304 (2009).

23. Lenrick, F., Ek, M., Deppert, K., Samuelson, L. & Reine Wallenberg, L. Straight and kinked InAs nanowire growth observed *in situ* by transmission electron microscopy. *Nano Res.* **7**, 1188–1194, DOI: https://doi.org/10.1007/s12274-014-0481-4 (2014).

24. Koivusalo, E. S. *et al.* Deterministic switching of the growth direction of self-catalyzed GaAs nanowires. *Nano Lett.* **19**, 82–89, DOI: https://doi.org/10.1021/acs.nanolett.8b03365 (2019).

25. Ostwald, W. Über die vermeintliche Isomerie des roten und gelben Quecksilberoxyds und die Oberflächenspannung fester Körper. *Z. Phys Chem.* **34U**, 495, DOI: https://doi.org/10.1515/zpch-1900-3431 (1900).

26. Pimpinelli, A. & Einstein, T. L. Capture-zone scaling in island nucleation: universal fluctuation behavior. *Phys. Rev. Lett.* **99**, 226102, DOI: https://doi.org/10.1103/PhysRevLett.99.226102 (2007).

27. Pimpinelli, A., Tumbek, L. & Winkler, A. Scaling and exponent equalities in island nucleation: novel results and application to organic films. *J. Phys. Chem. Lett.* **5**, 995–998, DOI: https://doi.org/10.1021/jz500282t (2014).

28. Haberern, K. W. & Pashley, M. D. GaAs(111)A–(2×2) reconstruction studied by scanning tunneling microscopy. *Phys. Rev. B* **41**, 3226–3229, DOI: https://doi.org/10.1103/PhysRevB.41.3226 (1990).

29. Shapiro, J. N., Lin, A., Huffaker, D. L. & Ratsch, C. Potential energy surface of In and Ga adatoms above the (111)A and (110) surfaces of a GaAs nanopillar. *Phys. Rev. B* **84**, 085322, DOI: https://doi.org/10.1103/PhysRevB.84.085322 (2011).

30. Brusaferri, L. *et al.* Thermally activated carrier transfer and luminescence line shape in self-organized InAs quantum dots. *Appl. Phys. Lett.* **69**, 3354–3356, DOI: https://doi.org/10.1063/1.117304 (1996).

31. Kissel, H. *et al.* Size distribution in self-assembled InAs quantum dots on GaAs (001) for intermediate InAs coverage. *Phys. Rev. B* **62**, 7213–7218, DOI: https://doi.org/10.1103/PhysRevB.62.7213 (2000).

32. Lee, S., Noh, S., Choe, J. & Kim, E. Evolution of bimodal size-distribution on InAs coverage variation in as-grown InAs/GaAs quantum-dot heterostructures. *J. Cryst. Growth* **267**, 405–411, DOI: https://doi.org/10.1016/j.jcrysgro.2004.04.014 (2004).

33. Debnath, M. C. *et al.* Optical properties of bimodally distributed InAs quantum dots grown on digital $AlAs_{0.56}Sb_{0.44}$ matrix for use in intermediate band solar cells. *J. Appl. Phys.* **121**, 214304, DOI: https://doi.org/10.1063/1.4984832 (2017).

34. Medeiros-Ribeiro, G., Bratkovski, A. M., Kamins, T. I., Ohlberg, D. A. A. & Williams, R. S. Shape transition of germanium nanocrystals on a ailicon (001) surface from pyramids to domes. *Science* **279**, 353–355, DOI: https://doi.org/10.1126/science.279.5349.353 (1998).

35. Daruka, I., Tersoff, J. & Barabási, A.-L. Shape transition in growth of strained islands. *Phys. Rev. Lett.* **82**, 2753–2756, DOI: https://doi.org/10.1103/PhysRevLett.82.2753 (1999).

36. Hopkins, B. & Skellam, J. G. A new method for determining the type of distribution of plant individuals. *Annals Bot.* **18**, 213–227, DOI: https://doi.org/10.1093/oxfordjournals.aob.a083391 (1954).

37. Konishi, T., Bell, G. R. & Tsukamoto, S. Hopkins-Skellam index and origin of spatial regularity in InAs quantum dot formation on GaAs(001). *J. Appl. Phys.* **117**, 144305, DOI: http://dx.doi.org/10.1063/1.4917213 (2015).

38. Horikoshi, Y., Uehara, T., Iwai, T. & Yoshiba, I. Area selective growth of GaAs by migration-enhanced epitaxy. *Phys. Status Solidi (b)* **244**, 2697–2706, DOI: https://doi.org/10.1002/pssb.200675621 (2007).

39. Ritzmann, J. *et al.* Overcoming Ehrlich-Schwöbel barrier in (111)A GaAs molecular beam epitaxy. *J. Cryst. Growth* **481**, 7–10, DOI: https://doi.org/10.1016/j.jcrysgro.2017.10.029 (2018).

40. Tsukamoto, S. & Koguchi, N. Magic numbers in Ga clusters on GaAs(001) surface. *J. Cryst. Growth* **209**, 258–262, DOI: https://doi.org/10.1016/S0022-0248(99)00551-5 (2000).

41. Nothern, D. M. & Millunchick, J. M. Template-dependent nucleation of metallic droplets. *J. Vac. Sci. Technol. B* **30**, 060603, DOI: https://doi.org/10.1116/1.4754563 (2012).

Acknowledgements

This research was funded by the European Union's Horizon 2020 research and innovation programme under the Marie Skłodowska-Curie grant agreement # 721394.

We thank Tommaso Radaelli, Stefania Riva, and Marta Tonini for the help in the data analysis.

Author contributions statement

S. S. and A. T. conceived the experiments. A. T., A. F., and S. B. carried out the sample growth and performed AFM measurements. A. T. performed the island nucleation analysis and the CZD analysis. R. T., S. V., and S. T. performed the Hopkins-Skellam analysis. All authors discussed the results and wrote the manuscript.

Competing interests

The authors declare no competing interests.

Data Availability

The datasets generated during and/or analysed during the current study are available from the corresponding author on reasonable request.

Figures

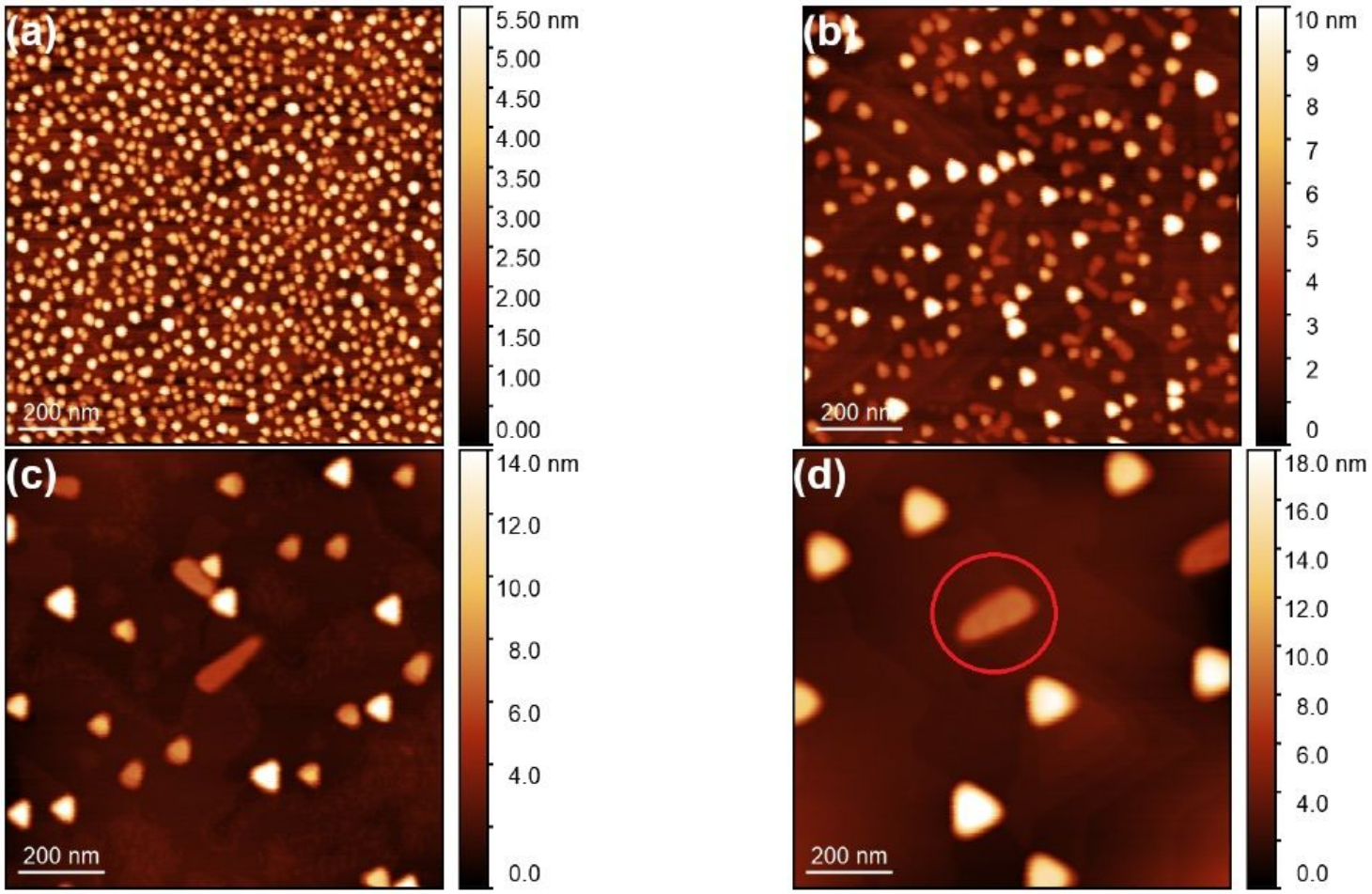

Figure 1

AFM topography images of GaAs islands grown on the GaAs(111)A substrate at (a) 300 C (1x1 mm2, sample T1); (b) 350 C (1x1 mm2, sample T2); (c) 400 C (1x1 mm2, sample T3); (d) 450 C (1x1 mm2, sample T4). The red circle highlights a kinked island.

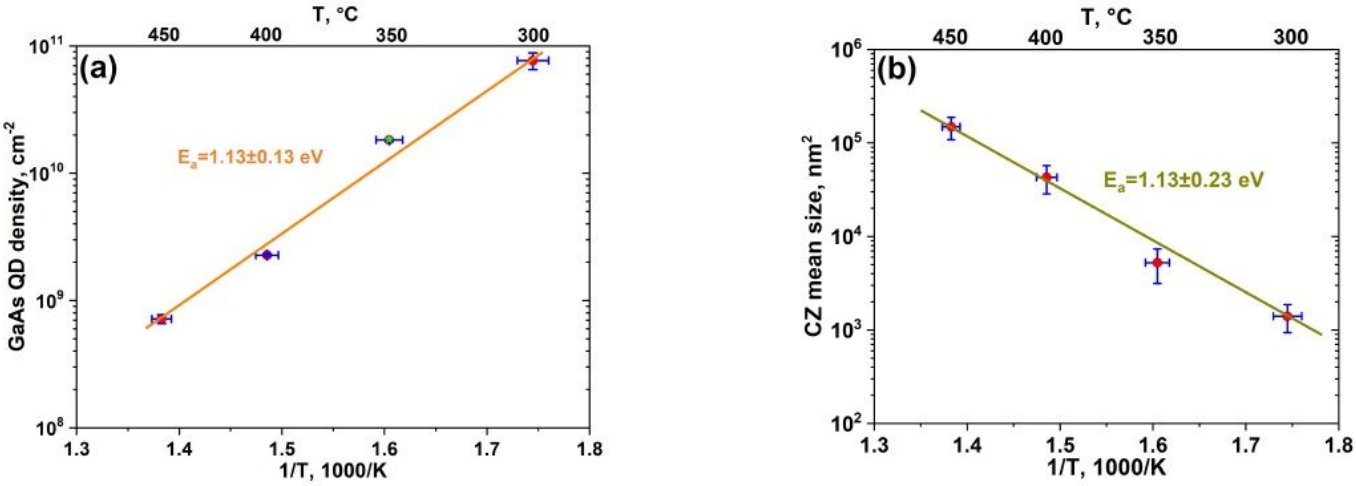

Figure 2

(a) The temperature density dependence of DE GaAs islands grown on GaAs(111)A substrate. The green star indicates the island density of the sample T2b. The nucleation activation energy, Ea = 1.13+0.13 eV. (b) The temperature dependence of a mean size of Voronoi cells. The activation energy Ea, calculated from this method, equals 1.13+0.23 eV. The temperature error bar for both graphs is +5 C.

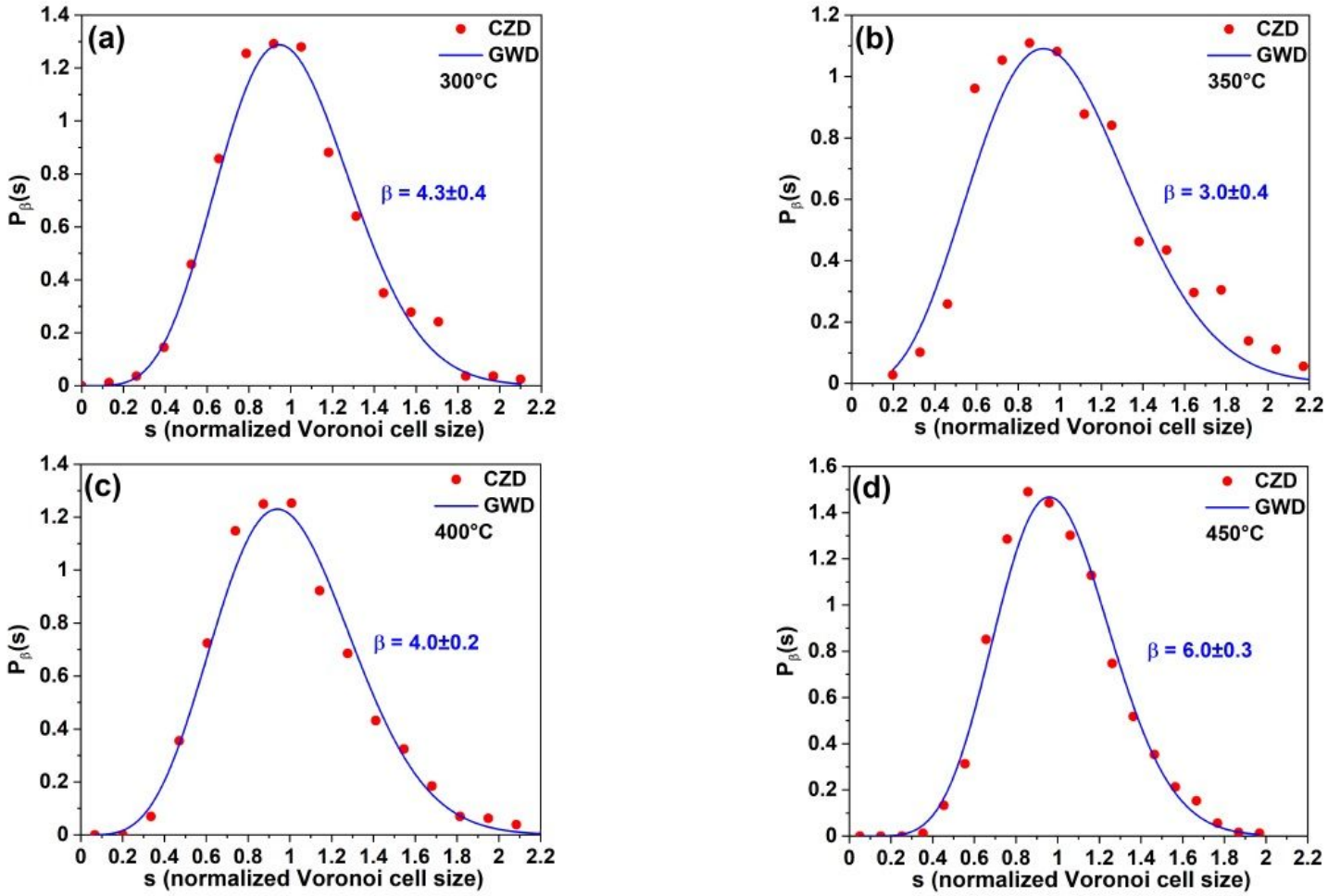

Figure 3

CZDs of the samples (a) T1, (b) T2, (c) T3, and (d) T4, fitted by the GWD.

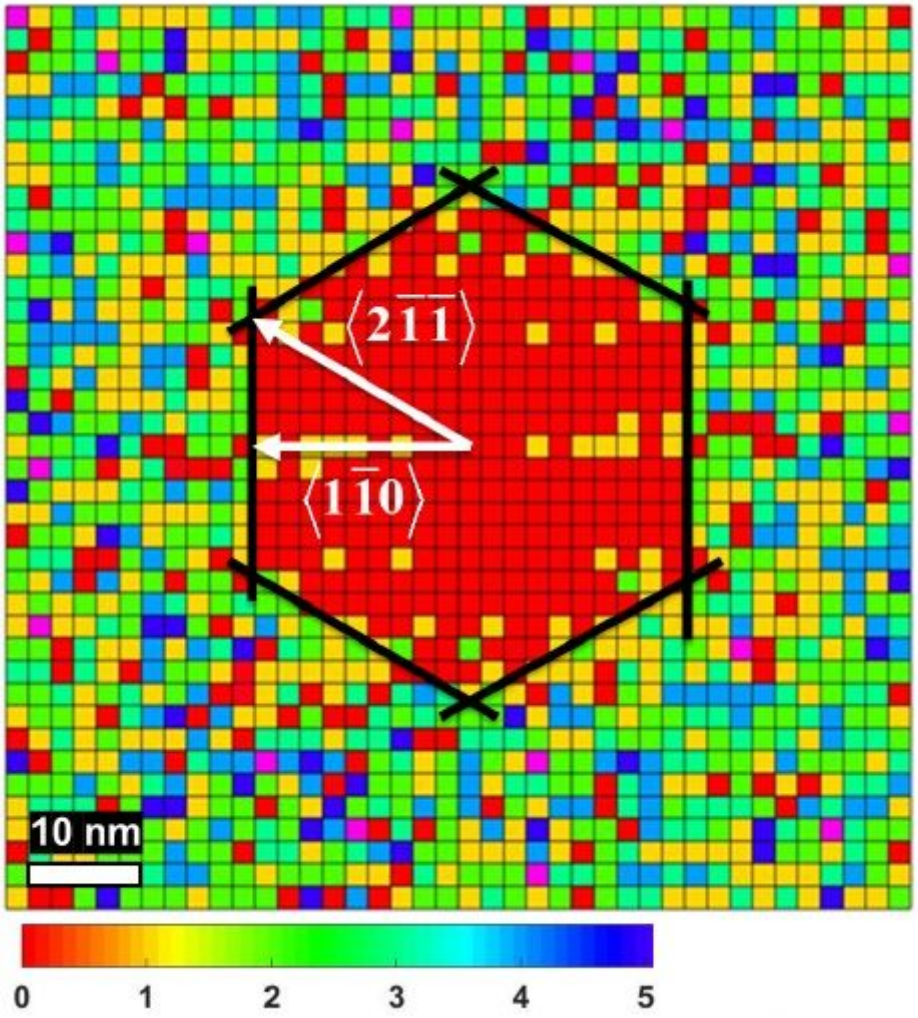

Figure 4

The spatial neighbor distribution of GaAs islands for the sample T1 (80x80 nm2).

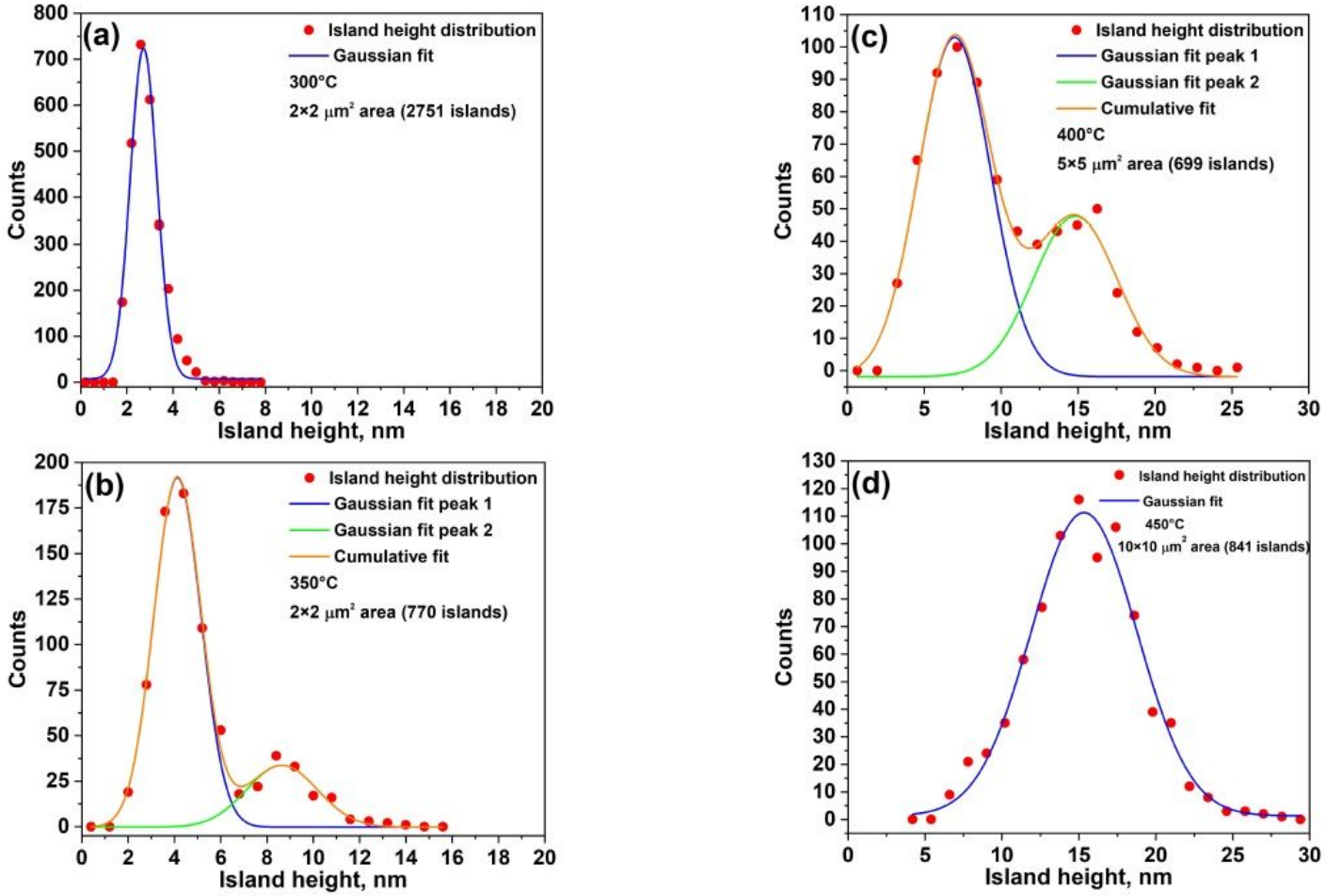

Figure 5

The GaAs island height distribution of samples (a) T1, (b) T2, (c) T3, and (d) T4. For the samples T1 and T4 an unimodal distribution is observed with a standard deviation of about 44%. The samples T2 and T3 have a bimodal distribution.

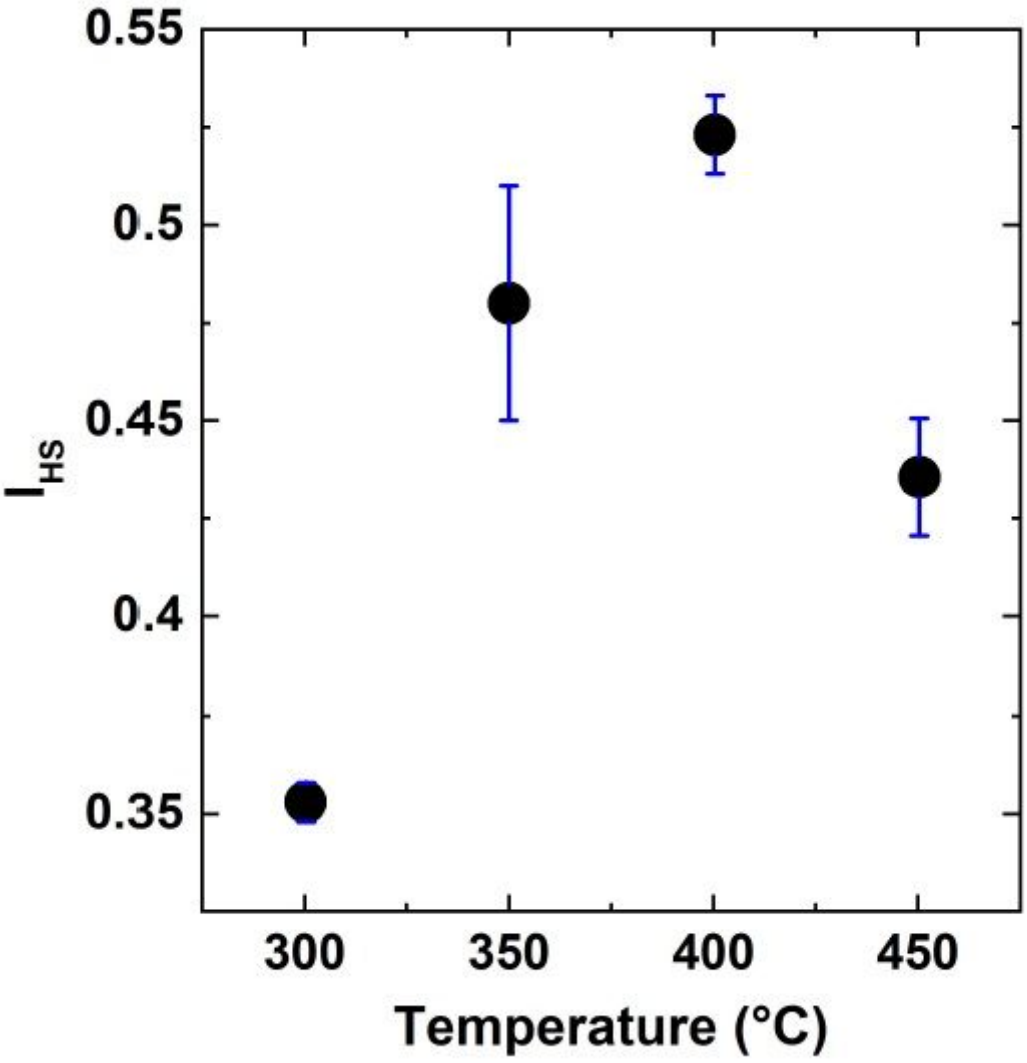

Figure 6

The dependence of the Hopkins-Skellam index (IHS) on the deposition temperature.

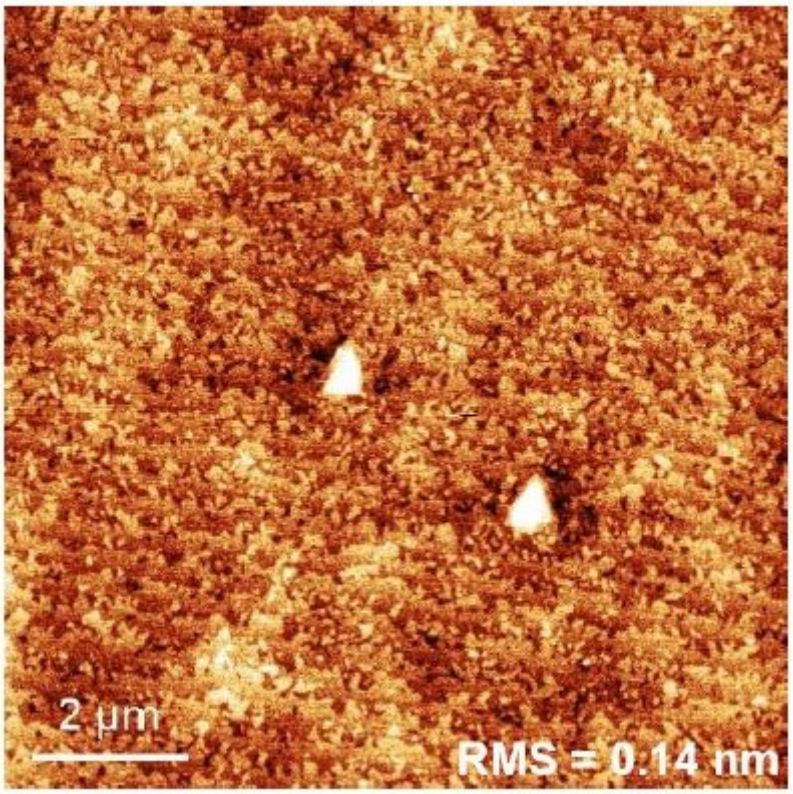

Figure 7

10x10 mm2 AFM amplitude image of GaAs buffer layer morphology, grown according to Ref.17 and used in this work.

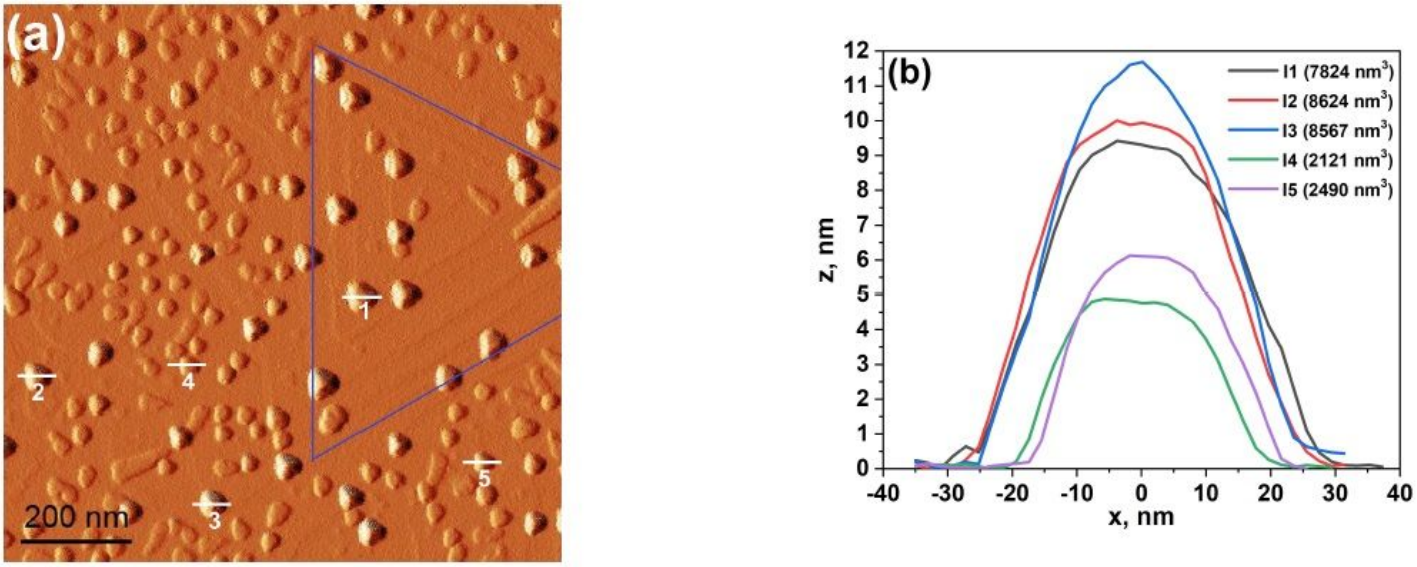

Figure 8

(a) 1x1 mm2 AFM amplitude image of the sample T2. The white lines indicate where the height profiles of islands were measured. The blue lines indicate the area of the stepped hillock. (b) The height profiles

of 5 islands of the sample taken from (a).